Genetic Algorithm Based Shape Optimization Method of DC Solenoid Electromagnetic Actuator

Eduard Plavec [1], Ivo Uglešić [2], and Mladen Vidović [1]

[1] Switchgear and Controlgear Department
KONČAR Electrical Engineering Institute, Inc., Zagreb, 10 000, Croatia
eplavec@koncar-institut.hr, mvidovic@koncar-institut.hr

[2] Department of Energy and Power Systems
Faculty of Electrical Engineering and Computing, Zagreb, 10 000, Croatia
ivo.uglesic@fer.hr

***Abstract* ─** This paper presents the method for the shape optimization of the DC solenoid electromagnetic actuator using a genetic algorithm. Numerical simulation of its transient response includes simultaneously solving differential equations of magnetic, electrical and mechanical subsystems. The magnetic subsystem is analyzed by finite element method (FEM), while the electrical and mechanical subsystems are modeled separately and mutually coupled. A modified genetic algorithm is programmed in MATLAB software package. The shape optimization has been performed on two-dimensional (2D) axial-symmetric model of electromagnetic actuator. The measurement results obtained after the production and testing of electromagnetic actuator are compared with results of numerical simulation.

***Index Terms* ─** Electromagnetic actuator, finite element method, genetic algorithm, shape optimization, solenoid.

I. INTRODUCTION

Solenoid electromagnetic actuators are electromechanical devices which convert electrical energy to mechanical energy related to linear motion. They are characterized by their compact size and simple structure, and due to their reliability, simple activation and cheap production, they are widely used in many components that accompany our daily lives [1,2].

The design of solenoid electromagnetic actuators (EMA) starts with operating conditions of the device. DC electromagnetic actuators usually do not have a linear static characteristic, but it can be achieved by the coil current control or by changing the shape of the magnetic circuit [3]. The current control is usually not the simplest way as it requires sophisticated sensors, a microcomputer and various electronic components. A more suitable way is to adjust the electromagnetic device's magnetic conductive parts shape. This does not lead to a completely linear characteristic of plunger movement, but it can be considered as satisfactory [4].

The shape influence of magnetic conductive parts of EMA-s was studied by Roters [5] even in the forties of the last century. The development of optimization methods began with the development of computer technology [6]. Unlike the local optimization techniques, evolutionary algorithms, like GA, are not highly dependent on either initial conditions nor on constraints in the solution domain [7]. Evolutionary algorithms attempt to imitate nature, where all living organisms exist in a given environment [8]. This idea can be modified and used for optimization problem solutions based on numerical calculations, assuming that the environment is defined on known values and characteristics [9,10].

There are a lot of different techniques used for the shape optimization of electromagnetic devices, but the usage of GA for shape optimization of electromagnetic actuators exist only in a few references which are listed below. The shape optimization of the electromagnetic valve with fixed permanent magnet using a GA is shown in [11], while in [12] it is used in similar application for the multi-objective optimization of electromagnetic components.

This paper presents the shape optimization method of DC EMA. The numerical simulation of the transient response of EMA includes simultaneously solving differential equations of magnetic, electrical and mechanical subsystems. Numerical calculations are performed using the ANSYS Electronics software package which consists of several modules. The magnetic subsystem is analyzed by finite element method (FEM) using ANSYS Maxwell, while the electrical and mechanical subsystems are separately modeled in the ANSYS Simplorer and mutually coupled. The GA is programmed in a MATLAB software package and linked to ANSYS Maxwell, where the electromagnetic

calculations have been performed on 2D axial-symmetric model.

The main advantage of the method presented in this paper is the possibility of the optimization electromagnetic force acting on plunger at specific plunger displacement, which could be very useful in many different applications of EMA-s.

II. DESCRIPTION AND WORK PRINCIPLE

The basic structure of the solenoid EMA consists of a non-magnetic shaft, sleeve bearing, upper and lower core, magnetic conductive housing, non-magnetic part of housing, coil, working gap, plunger and return spring (Fig. 1).
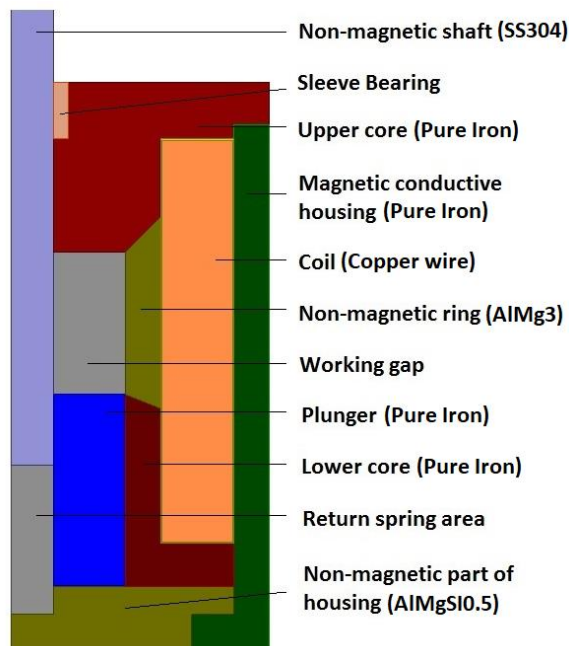

Fig. 1. DC solenoid electromagnetic actuator – basic structure (cross-section).

The non-magnetic shaft separates the magnetically conductive parts (cores and plunger) and transfers the mechanical force of the plunger to a certain mechanism that the electromagnetic actuator starts. The key role of sleeve bearing is to reduce sliding friction between the magnetic conductive upper core and the movable non-magnetic shaft. The stationary ferromagnetic core as well as the movable ferromagnetic plunger are the basic parts of the actuator through which the magnetic circuit closes. The cores, housing and plunger are made of electrically conductive material with non-linear B-H characteristics. The original purpose of the non-magnetic ring is to act like a plunger guide tube and to prevent its eccentric force, offering a smooth sliding surface with a low friction sliding coefficient. If the non-magnetic ring

is located in the middle of the coil it can also increase the operating speed of the plunger [13]. The working gap, in some references also known as the main air gap, is the place where attraction force between the plunger and the core is generated, i.e., the place of electromechanical conversion of energy. The function of the return spring is to return the plunger to its initial position after switching off the EMA. The purpose of the non-magnetic part of the housing is to determine the initial position of the plunger.
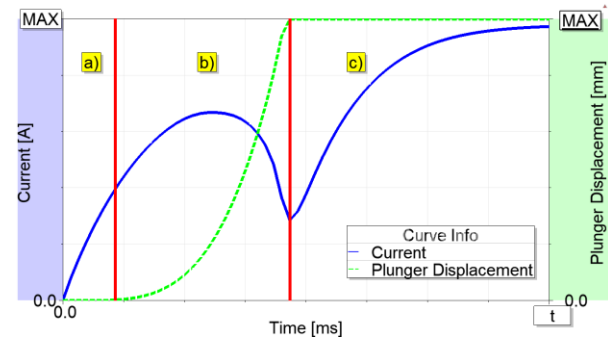

Fig. 2. The typical response behavior of the DC solenoid electromagnetic actuator.

The typical response behavior of DC EMA is illustrated in Fig. 2 and consists of the following three operation periods [14], mutually separated with red vertical lines:

a) The Sub-transient Period. In this period the plunger does not move, it is at rest despite the application of excitation voltage. The magnetic flux which flows through the plunger does not raise simultaneously with magnetomotive force (MMF) due to the presence of eddy currents.

b) The Transient Period. This period starts when the electromagnetic force of the plunger becomes larger than the initial return spring force and therefore the plunger starts to move. The movement of the plunger causes the varying magnetic flux in the EMA. The electromotive force (EMF), which opposes to the voltage source and causes the current drop, is induced in the coil due to change of linkage magnetic flux.

c) The Stopping Period. In this mode, the plunger touches the upper part of the core and finishes the movement, the EMF disappears and current continues to increase.

The EMA that should be optimized starts the newly developed high-voltage circuit breaker mechanism. It should overcome the force of 80 N at the plunger displacement of 6 mm and meet all the design constraints which are listed in Table 1. The mechanism's built–in switches are capable of breaking the current in the amount of 2.5 A.

Table 1: Design constraints parameters of EMA

Design Constraint Parameter	Value
Max. current	2.5 A
Electromagnetic force	>80 N (6 mm)
Actuator width	<60 mm
Actuator height	<70 mm
Plunger displacement	10 mm
Voltage supply	220 VDC

III. MATHEMATICAL MODEL

Dynamic modeling of the time response of the electromagnetic actuator is difficult because of the need to simultaneously solve non-linear differential equations of its magnetic, electrical and mechanical subsystem [15]. The equations which lead to time and space dependent electromagnetic magnitudes and which are also used to solve the magnetic subsystem of electromagnetic actuator are well known Maxwell's equations [16,17]:

$$div\vec{B} = 0, \tag{1}$$
$$rot\vec{H} = \overrightarrow{J_{EC}} + \vec{J}, \tag{2}$$
$$rot\vec{E_\iota} = -\frac{\partial \vec{B}}{\partial t}, \tag{3}$$
$$\overrightarrow{J_{EC}} = \sigma \cdot \vec{E_\iota}, \tag{4}$$
$$\vec{B} = \mu \cdot \vec{H}, \tag{5}$$

with the following notations: $\vec{B}$ – magnetic flux density and $\vec{H}$ – magnetic field strength, $\vec{J}$ – current density, $\overrightarrow{J_{EC}}$ – eddy current density, $\vec{E_\iota}$ – induced electric field strength, μ – permeability of material and σ – conductivity of material. To solve these equations in the case of axial-symmetric geometry, it is convenient to use the magnetic vector potential defined as:

$$\vec{B} = rot\vec{A}. \tag{6}$$

By combining the Equations (2), (4), (5) and (6) the following equations are obtained:

$$\vec{B} = \mu \cdot \vec{H} = rot\vec{A} \rightarrow H = B/\mu, \tag{7}$$
$$rot(\vec{B}/\mu) = \sigma \cdot \vec{E_\iota} + \vec{J}. \tag{8}$$

Furthermore, if we put expression (6) into the Equation (3) the following equation is obtained:

$$rot\vec{E_\iota} = -\frac{\partial \vec{B}}{\partial t} = -\frac{\partial(rot\vec{A})}{\partial t} \rightarrow \vec{E_\iota} = -\frac{\partial \vec{A}}{\partial t}, \tag{9}$$
$$rot\left(\frac{rot\vec{A}}{\mu}\right) = -\sigma \cdot \frac{\partial \vec{A}}{\partial t} + \vec{J}. \tag{10}$$

In the case of axial-symmetric geometry, the vector potential $\vec{A}$ has only one component and that scalar function depends on two space variables (r, z) and time (t). The final expression for the time dependable differential equation of magnetic subsystem, with implementation of all causes of eddy currents is [1]:

$$\frac{\partial}{\partial z}\left(\frac{1}{\mu} \cdot \frac{\partial \vec{A}}{\partial z}\right) + \frac{\partial}{\partial r}\left(\frac{1}{\mu} \cdot \frac{1}{r} \cdot \frac{\partial(r \cdot \vec{A})}{\partial r}\right) = \sigma \cdot \frac{\partial \vec{A}}{\partial t} - \vec{J}. \tag{11}$$

This equation should be solved taking into consideration the boundary condition $(\overrightarrow{A_z} = 0)$ in reference to the system of stationary and movable parts of the EMA. The electric subsystem is composed of coil and DC power supply. The applied voltage U is given as a function of current and time and can be expressed, after the simplification of the linkage flux expression, with the following differential equation:

$$\lambda = N \cdot \Phi = NBS = N \cdot \mu_0 \frac{N \cdot i}{h} \cdot S = L \cdot i, \tag{12}$$
$$(R_i + R_Z) \cdot i(t) + \frac{d\lambda(i,z)}{dt} = U(t), \tag{13}$$

with the following notations: λ – linkage magnetic flux, N – number of turns, Φ – magnetic flux, B – magnetic flux density, S – cross section area of coil, i – coil current, h – height of coil, R_i – resistance of power supply, R_z – resistance of coil, U – applied voltage.

The position of movable plunger is defined by the following equation of motion:

$$m\frac{d^2z}{dt} + \gamma\frac{dz}{dt} + kz = F_e - F_R, \tag{14}$$

where γ and k are friction and stiffness coefficients. F_e and F_R are electromagnetic force and friction force, while m is the mass of the plunger. The model of all three subsystems are mutually coupled in the ANSYS Electronics software package, as it is shown in Fig. 3.
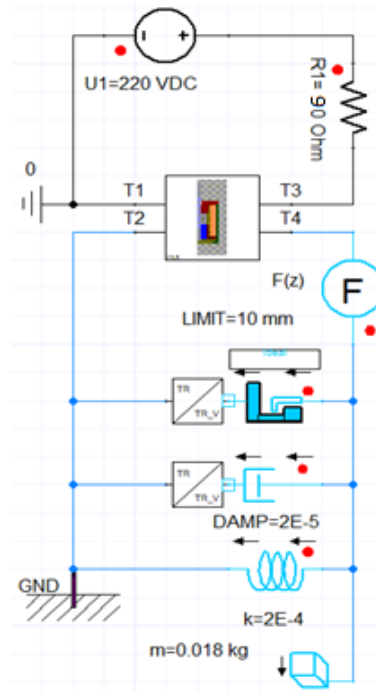

Fig. 3. The model of DC solenoid EMA in ANSYS Electronics.

The electromagnetic force acting on the plunger in dependence on plunger displacement, is obtained as follows. Coil width can be calculated using following equation:

$$w_c = N_x \cdot D_w, \tag{15}$$

where N_x is, the number of turns in x direction and D_w is wire diameter. To calculate the coil height, the Pappus

centroid theorem for volume of solids of revolution is used:

$$V = 2\pi \cdot A \cdot d = L \cdot A_w = \frac{R}{R_{lin}} \cdot A_w, \qquad (16)$$

where A is, the area of the surface which is rotating, d is the distance of its geometric centroid from the axis of revolution, L is the length of wire, A_w is the area of the wire cross section, R is the coil resistance and R_{lin} is the linear resistance. The distance and area can be obtained using equations:

$$d = w_c + r_{po} + t_{lc}, \qquad (17)$$

$$A = N_x \cdot N_y \cdot A_w, \qquad (18)$$

$$N_y = h_c / D_w, \qquad (19)$$

with the following notations: r_{po} – plunger outer radius, t_{lc} – lower core thickness, N_y – number of turns in y direction, h_c – coil height (Fig. 4). By combining the Equations (16), (17), (18) and (19) it is obtained the equation for calculation of the coil height:

$$h_c = \frac{D_w \cdot R}{\pi \cdot N_x \cdot R_{lin} \cdot (r_{po} + w_c + t_{lc})}. \qquad (20)$$

From the definition of Maxwell Stress Tensor and the properties of Kronecker delta with the fact that the magnetic field B has only y component, it is possible to write the force acting on plunger as:

$$\sigma_{yy} = \frac{1}{\mu_0} B_y B_y - \frac{1}{2\mu_0} B^2 \delta_{yy}, \qquad (21)$$

$$\sigma_{yy} = \frac{1}{\mu_0} B^2 - \frac{1}{2\mu_0} B^2 = \frac{B^2}{2\mu_0} = F, \qquad (22)$$

$$F_e(z) = \frac{\mu_0 (NI)^2 S}{2\left(\frac{l_m}{\mu_r} + z\right)^2}, \qquad (23)$$

where S is, the cross-section area of plunger, l_m is the length of the path along ferromagnetic material, μ_r is relative permeability of material and z is the plunger displacement. The cross-section area of the plunger can be obtained using equation:

$$S = \pi \cdot (r_{po}^2 - r_{nms}^2), \qquad (24)$$

where r_{nms} is the radius of non-magnetic shaft. Length of the path along the ferromagnetic material is calculated using the following equation:

$$l_m = 2r_{co} - 2r_{nms} + t_h + \frac{t_{lcb}}{2} + h_c + t_{lc} - \qquad (25)$$
$$r_{ci} + h_p + i_{lc} + i_{uc} + h_{uc},$$

with the following notations: r_{co} – coil outer radius, t_h – housing thickness, t_{lcb} – lower core base thickness, h_c – coil height, t_{lc} – lower core thickness, r_{ci} – inner coil radius, h_p – plunger height, h_{sb} – sleeve bearing height, i_{lc} – incline of lower core, i_{uc} – incline of upper core, t_{ucb} – upper core base thickness, (Fig. 4). If we combine Equations (15), (20), (22), (23), (28) and put it in Equation (21) the final expression for force acting on plunger is obtained.
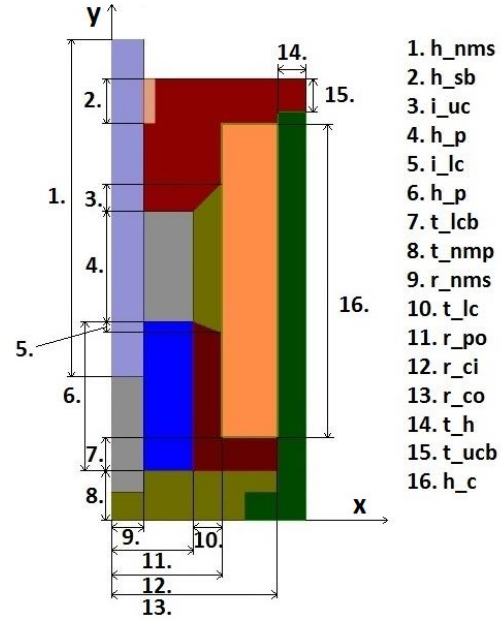

Fig. 4. Design variables overview.

IV. METHODOLOGY

The electromagnetic calculation is performed using the ANSYS Electronics software package, using its two modules, ANSYS Maxwell and ANSYS Simplorer. ANSYS is started in interactive mode (not batch mode), so if we have a repetitive task that just needs to change some parameters, there is no need to start up ANSYS for all studies, which saves up a lot of time and is very interesting when performing the optimization process.

The first step to link Maxwell with MATLAB is writing an ANSYS script in an ANSYS ADPL environment. The second step is creating a batch file to run ANSYS from MATLAB. The batch file is used for communication, to forward results of finite element analysis (FEA) to MATLAB and to return input parameters from MATLAB to ANSYS (Fig. 5).
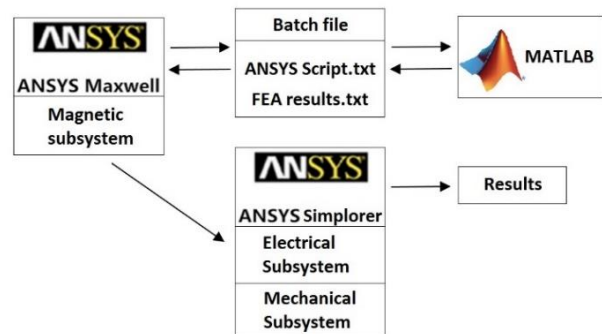

Fig. 5. Overview of computation methodology.

MATLAB performs the geometry generation calculations, the analysis required to suggest a geometry which approaches the optimal shape design of EMA, using the GA. The inputs to the GA are the design parameters, constraints and objectives that need to be maximized. The main parameters required by the GA (Table 2), such as the number of individuals to be analyzed, the mutation rate, crossover rate, the list of variables we are optimizing and the maximum number of iterations are declared in ANSYS script.

Table 2: The main parameters of GA

Number of Individuals	30
Crossover Rate	0.6
Mutation Rate	0.05
Crossover Type	Uniform
Mutation Type	Uniform
Maximum Number of Iterations	5000

The optimization process in MATLAB starts with a randomly generated population of design variables, with their initial values encoded as genes in a chromosome [18]. Once the population is initialized the operators are used to modify genes after which the fitness function is called [19]. As the design objective is to maximize force at a specific plunger displacement taking all the constraints into consideration, the fitness function converted to the minimization problem is:

$$\text{Fitness Funtion} = \text{Minimize}\left(\frac{1}{F_e(z)}\right). \quad (26)$$

At this point all the constraints are checked, objective values computed and ANSYS Maxwell module is provided with a shape of geometry. Numerical simulation results of magnetic subsystem of EMA-a are then forwarded to the ANSYS Simplorer where the subsystems are mutually coupled and results are obtained. This process is repeated until a stopping criterion is reached, which happens when the number of generations is reached or solution has converged (Fig. 6).

The seventeen design variables are selected to operate shape optimization of the presented EMA. The parts which are very sensitive to the change of reluctance, like the top end area of the plunger, have its shape separated with a few more sub-variables to achieve the most suitable shape as it is described in [1]. Due to the initial design constraint on plunger displacement it is possible to fix the working gap variable to the required value as well as neglect variables that have no effect on electromagnetic properties of EMA, it will speed up the optimization process.

Depending on the initial constraints on current and voltage supply it is possible to calculate coil resistance and parametrize coil. The inner coil radius is defined by the plunger outer radius and thickness of lower core:

$$r_{ci} = r_{po} + t_{lc}. \quad (27)$$

The outer coil radius is defined by coil resistance, wire diameter, bare wire diameter, coil height, winding stacking factor and the inner coil radius:

$$r_{co} = \sqrt{\frac{R \cdot D_{bw}^2 \cdot D_w^2}{4 \cdot \rho \cdot h_c \cdot p} + r_{ci}^2}, \quad (28)$$

$$D_{bw} = 0.0826 \cdot 1.123^{-AWG}, \quad (29)$$

$$D_w = 0.0082 \cdot 0.8931^{AWG}, \quad (30)$$

with the following notations: R – coil resistance, D_{bw} – bare wire diameter, ρ – resistivity, r_{ci} – coil inner radius, r_{co} – coil outer radius, D_w – wire diameter, h_c – coil height, p – winding stacking factor, AWG – American wire gauge. According to the references [6,7,18], the values of the winding stacking factor are in range from 0.65 to 0.8.
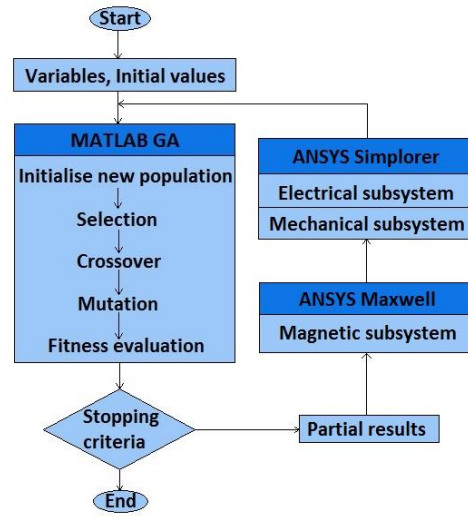

Fig. 6. Flow diagram of the optimization process.

V. ANALYSIS OF NUMERICAL RESULTS

The developed method has been applied to DC solenoid EMA with exciting external voltage as a step function (220 V). The optimization process had been performed on a PC with CPU Intel Core i7 (3.8 GHz, 16 cores) and 64 GB RAM. The solution converged after two weeks of calculation and 2348 generations (Fig. 7).

At the beginning of the transient phenomenon, the eddy currents, which oppose the magnetic field of coil by their magnetic field, are induced. This phenomenon is called magnetic diffusion and causes a penetration delay of the magnetic field in the interior of housing, cores and plunger, which adversely affects the response time of the EMA.

The magnetic diffusion phenomenon can be clearly seen in Fig. 8, where the distribution of the magnetic field in EMA at t=1.6 ms, t=4.6 ms and t=5.6 ms is illustrated. The magnetic flux in the working gap is distributed uniformly in the radial direction, while that is not the case with flux distribution on the pole face of the plunger (Fig. 9). This phenomenon is called the pole face effect [20]. The steady-state magnetic flux is not uniform

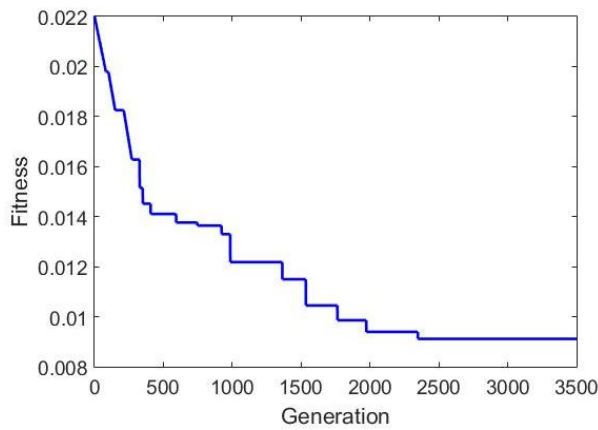due to the hysteresis effect of the magnetic core.
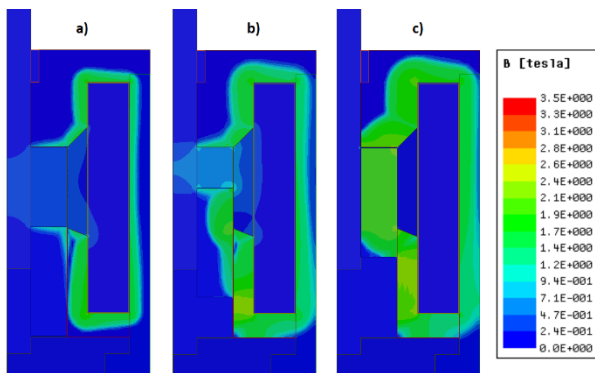

Fig. 7. Genetic algorithm convergence curve.

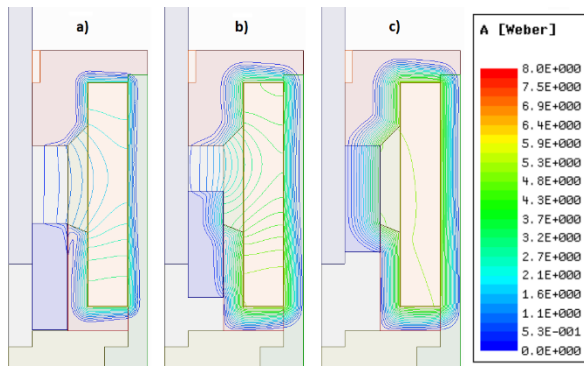Fig. 8. Dynamic distribution of magnetic field in the actuator at: (a) t=1.6 ms, (b) t=4.6 ms, and (c) t=5.6 ms.

Fig. 9. Dynamic flux distribution in the actuator at: (a) t=1.6 ms, (b) t=4.6 ms, and (c) t= 5.6 ms.

Numerical simulation results of the coil current, plunger displacement, speed, induced voltage and flux linkage are shown in Fig. 10 and Fig. 11 as functions of time.
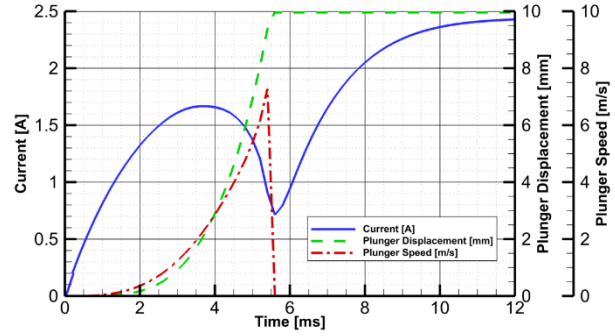

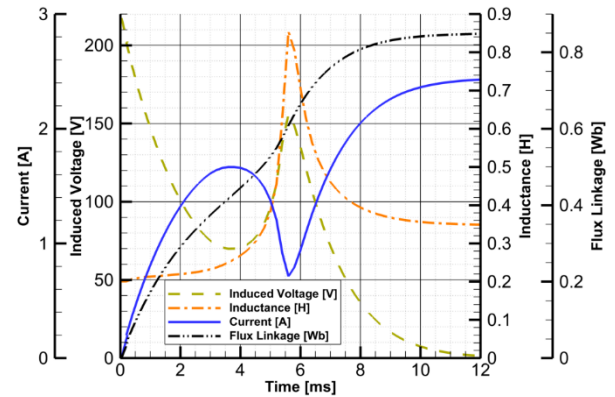Fig. 10. Numerical simulation results of solenoid EMA.

Fig. 11. Numerical simulation results (2) of solenoid EMA.

The plunger does not start to move until the magnetic flux penetrates into the plunger enough and electromagnetic force on the plunger overcomes the initial load force of spring (0.4 N). During the motion, the plunger reaches the maximum speed of 7.3 m/s. The time response of simulated EMA is 5.59 ms. The static values of electromagnetic force depending on the plunger displacement are obtained using the magnetostatic calculation. The results are shown in Fig. 12.
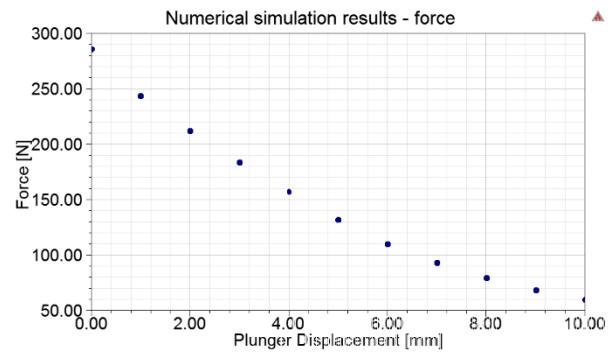

Fig. 12. Numerical simulation results of solenoid EMA, force characteristics.

At maximum plunger displacement, the static electromagnetic force has its minimum value of 59.7 N. As the plunger approaches the end of motion, the force continues to increase. The maximum static electromagnetic force is reached at the end of motion and its value is 285.1 N. Since the static value of electromagnetic force at plunger displacement of 6 mm is higher than 80 N, the initial design constraint is satisfied.

VI. MANUFACTURING, TESTING AND RESULTS COMPARISON

After completion of the optimization process, the 3D model of the most optimal shape of electromagnetic actuator and square fasten plate are modeled in SolidWorks, after which the prototype is sent to manufacturing. The final optimized values of design variables are stated in Table 3.

Table 3: Optimized values of design variables

	Design Variable	Range	Optimized Value
1.	h_{nms}	20-60 mm	50 mm
2.	h_{sb}	2-10 mm	4 mm
3.	i_{uc}	0-7 mm	4.4 mm
4.	z	10 mm	10 mm
5.	i_{lc}	0-5 mm	3.2 mm
6.	h_p	9-16 mm	15.2 mm
7.	t_{lcb}	2-5 mm	4.1 mm
8.	t_{nmp}	3 mm	3 mm
9.	r_{nms}	2-5 mm	2.5 mm
10.	t_{lc}	2-5 mm	2.2 mm
11.	r_{po}	2-15 mm	11.5 mm
12.	r_{ci}	5-20 mm	13.7 mm
13.	r_{co}	6-40 mm	16.0 mm
14.	t_h	2-5 mm	2.0 mm
15.	t_{ucb}	2-8 mm	2.8 mm
16.	h_c	10-50 mm	29.7 mm
17.	h_{uc}	10-25 mm	13.8 mm
18.	AWG	29-34	32

The prototype of the EMA, after the manufacturing process, had been tested in the laboratory. The measured sizes are: plunger displacement, electromagnetic force on the plunger, coil current and coil resistance. The coil resistance, measured using a standard multimeter (FLUKE 88V/A), is 87.5 Ω, which is slightly less than 3% to the simulated value. The transient recorder (National Instruments TR12K) with sample rate of 20 MS/s and its acquisition unit is used to measure fast transient phenomena precisely. The inductive LVDT sensor (induSENSOR DTA25), connected to the transient recorder's acquisition unit and attached to the non-magnetic shaft of EMA, is used to measure the plunger displacement. The prototype of EMA is fixed to the

testing unit using a non-magnetic material not to affect the magnetic field of EMA. The test configuration is illustrated in Fig. 13.
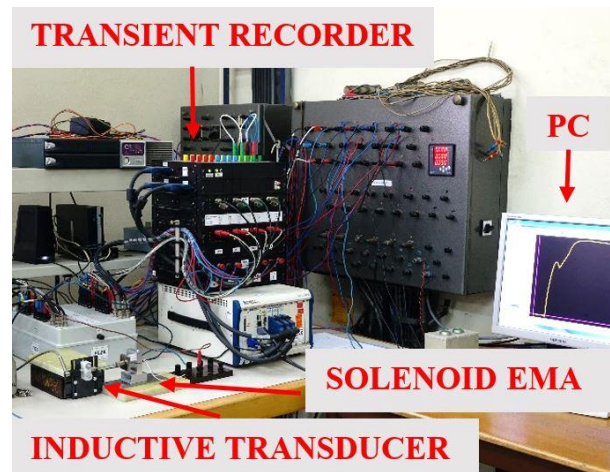

Fig. 13. Testing of prototype EMA.

The comparison of the numerical simulation results and the measurement results of the plunger displacement and coil current, are illustrated in Fig. 14.
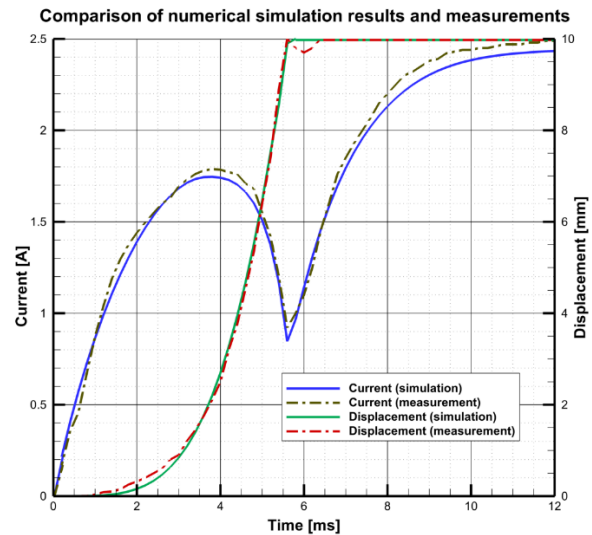

Fig. 14. Comparison of numerical simulation results and measurements.

The measured time response of tested EMA is 5.5 ms, which is 1.6% less than the numerical simulation response. The maximum deviation between the calculated and measured values of the coil current is 4%, while the maximum deviation between calculated and measured values of plunger displacement is 5%. The reasons the simulated results of coil current are smaller than measured results are the difference in calculated and measured coil

resistance and neglection of friction between the sleeve bearing and the non-magnetic shaft. The maximum deviation of simulated results and measurements of plunger displacement is obtained at the end of motion, when plunger rebounds.

The force measurement is conducted using a previously mentioned testing unit, but instead of inductive sensor the spring with known characteristic is used. The force is measured in nine points, repeatedly at every 1 mm of distance between solenoid EMA and testing unit. Based on the spring characteristics and its compression, the force that EMA has to overcome at specific distance is calculated. If the force amount is too large, the same is decreased to the level which EMA can overcome. The test configuration can be seen in Fig. 15.

Fig. 15. Force measurement test configuration.

The force measurement of this type gives the static values of electromagnetic force at specific distance and is not comparable to the dynamic electromagnetic force of transient numerical simulation. In order to compare transient numerical simulation results of the electromagnetic force with the measurements, magnetostatic calculation is performed with current values that correspond to forces for specific values of distance between the EMA and the testing unit. A comparison of numerical simulation results and force measurements are shown in Fig. 16.
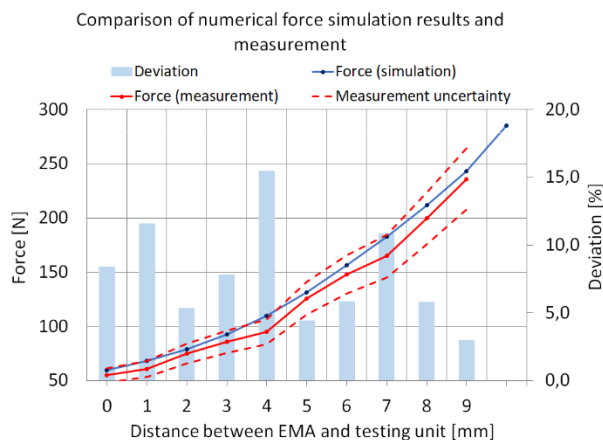

Fig. 16. Comparison of numerical force simulation results and measurement.

The maximum measured value of the static electromagnetic force, at the distance between the EMA and the testing unit of 9 mm, is 236 N. The static electromagnetic force measured at a plunger displacement of 6 mm is 149.8 N and it satisfies the initial design constraint. The maximum deviation between the calculated and measured values of the static electromagnetic force is 16.1%, at a distance between the EMA and the testing unit of 4 mm. At the same time, this measurement point is the only point which is outside the uncertainty zone ($\pm$12%) of force measurement unit. The main reason for this deviation is insufficiently precise force measurement method which should be improved on in further work.

The prototype model of the EMA (Fig. 17) has radius of 18 mm, while its overall height is 47 mm, which meets the initial design constraints (Table 1) on the actuator width and height. Compared to the initial design which is developed in the late nineties, the optimized design has smaller dimensions and a faster time response. Using the described optimization method electromagnetic force has increased during the plunger motion, while the maximum force at the end of motion is 5.93% less than initial design (Table 4). Since the effective working range of both EMA-s is between 6 and 8 mm of the plunger displacement, the maximum force at the end of motion is not so important.
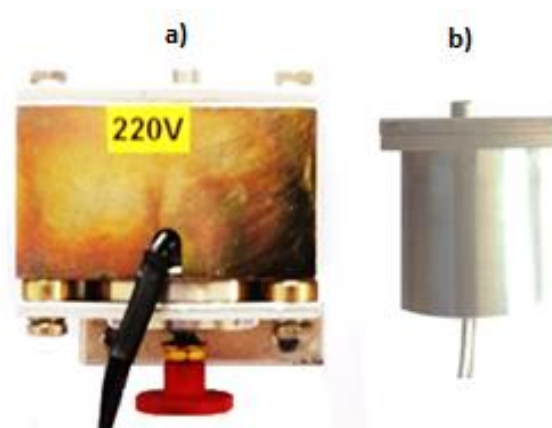

Fig. 17. Design of EMA-s: (a) initial and (b) optimized.

Table 4: Comparison of initial and optimized model of EMA

	Initial Design	Optimized Design	Improvement
Height [mm]	80	47	**-41.25%**
Width [mm]	63	36	**-42.86%**
F_{MAX} [N]	250	236	**-5.6%**
$F(6\ mm)$ [N]	114	156	**+36.84%**
Time response [ms]	8	5.6	**-30%**

VII. CONCLUSION

Electromagnetic actuators (EMA-s) which start some kind of tripping mechanism usually need a certain force value at specified plunger displacement to overcome the initial force of tripping mechanism. Maximizing the electromagnetic force during the time response usually results with a maximized electromagnetic force at the end of motion, in the saturation area, which is not very useful in this case. In this paper, the shape optimization method of the EMA-s which is based on a genetic algorithm and the finite element method, with the added ability to maximize electromagnetic force at desired plunger displacement, is presented.

After completion of the optimization process, the EMA with the most optimal shape is produced and tested in laboratory. The presented optimization method of the EMA gives the simulation results with a maximum deviation of 4% compared to the measured values of coil current and 5% compared to measured values of plunger displacement. The maximum deviation between force measurements and simulated results are 16.1% due to the insufficiently precise force measurement method, which needs to be improved. Using the presented optimization method, the achieved electromagnetic force acting on the plunger at a plunger displacement of 6 mm is 157 N, which is an improvement of 36.84% compared to the initial model of EMA. Also, based on this method, the dimensions of EMA are reduced 70.2% in height and 75% in width.

Based on the obtained results, it can be concluded that this method can successfully optimize the shape and describe the dynamic behavior of EMA-a and therefore be used for the design and development of such systems.

REFERENCES

[1] E. Plavec and M. Vidović, "Genetic algorithm based plunger shape optimization of DC solenoid electromagnetic actuator," *24th Conf. IEEE TELFOR 2016*, Belgrade, 2016.

[2] D. Cvetković, I. Ćosić, and A. Šubić, "Improved performance of the electromagnetic fuel injector solenoid actuator using a modelling approach," *International Journal of Applied Electromagnetics and Mechanics*, vol. 27, pp. 251-273, IOS Press, 2008.

[3] S.-B. Yoon, J. Hur, Y.-D. Chun, and D.-S. Hyun, "Shape optimization of solenoid actuator using the finite element method and numerical optimization technique," *IEEE Trans. Mag.*, vol. 33, Sept. 1997.

[4] T. Glück, *Soft Landing and Self-sensing Strategies for Electromagnetic Actuators*, ISSN 1866-2242, Shaker Verlag, Aachen, 2013.

[5] H. C. Roters, *Electromagnetic Devices*, New York, 1941.

[6] F. Mach, I. Novy, P. Karban, and I. Doležel, "Shape optimization of electromagnetic actuators," *IEEE Conf. ELEKTRO*, pp. 595-598, 2014.

[7] O. G.Bellmunt and L. F.Campanile, *Design Rules for Actuators in Active Mechanical Systems*, Springer, New York, 2010.

[8] H. R. E. H. Bouchekara and M. Nahas, "Optimization of electromagnetics problems using an improved teaching-learning-based-optimization technique," *ACES Journal*, vol. 30, no. 12, Dec. 2015.

[9] R. Diaz de Leon-Zapata, G. Gonzalez, A. G. Rodriguez, E. Flores-Garcia, and F. J. Gonzalez, "Genetic algorithm for geometry optimization of optical antennas," *Proceedings of the COMSOL Conference*, Boston, 2016.

[10] S. M. Makouie and A. Ghorbani, "Comparison between genetic and particle swarm optimization algorithms in optimizing ships' degaussing coil currents," *ACES Journal*, vol. 31, no. 5, May 2016.

[11] S. H. Lee, H. C. Yi, K. Han, and J. H. Kim, "Genetic algorithm-based design optimization of electromagnetic valve actuators in combustion engines," *ENERGIS*, vol. 8, pp. 13222-13230, 2015.

[12] A. Subbiah and O. Ladin, "Genetic algorithm based multi-objective optimization of electromagnetic components using COMSOL® and MATLAB®," *COMSOL Conference Proceedings*, Boston, 2016.

[13] J. S. Ryu, Y. Yao, C. S. Koh, S. N. Yun, and D. S. Kim, "Optimal shape design of 3D nonlinear electromagnetic devices using parametrized design sensitivity analysis," *IEEE Trans. Mag.*, vol. 41, no. 5, 2005.

[14] R. Narayanswamy, D. P. Mahajan, and S. Bavisetti, "Unified coil solenoid actuator for aerospace application," *Electrical Systems for Aircraft, Railway and Ship Propulsion (ESARS), IEEE*, 2012.

[15] M. Hassani and A. Shoulaie, "Dynamic modeling of linear actuator using fuzzy system to approximate magnetic characteristics," *ACES Journal*, vol. 30, no. 8, Aug. 2015.

[16] D. Jiles, *Introduction to Magnetism and Magnetic Materials*, CRC Press, 2016.

[17] M. Lahdo, T. Ströhla, and S. Kovalev, "Magnetic propulsion force calculation of a 2-DOF large stroke actuator for high-precision magnetic levitation system," *ACES Journal*, vol. 32, no. 8, Aug. 2017.

[18] S. R. B. Rama and D. Vakula, "Optimized polygonal slit rectangular patch antenna with defective ground structure for wireless applications," *ACES Journal*, vol. 30, no. 11, Nov. 2015.

[19] G. Liu, Y. Wang, X. Xu, W. Ming, and X. Zhang, "The optimal design of real time control precision of planar motor," *ACES Journal*, vol. 32, no. 10, Oct. 2017.

[20] K. Bessho and S. Yamada, "Analysis of transient characteristics of plunger-type electromagnets," *Electrical Engineering in Japan*, vol. 82, no. 4, 1978.

Eduard Plavec was born in 1988, in Zagreb, Croatia. He is a Ph.D. student at University of Zagreb, Faculty of Electrical Engineering and Computing where he also received his B.Sc. and M.Sc. degrees in Electrical Engineering and Information Technology in 2011 and 2013, respectively.

He joined KONČAR Electrical Engineering Institute in 2014, where he began as a Research and Development Engineer in the field of electromagnetics at the Switchgear and Controlgear Department. His areas of interest include computational electromagnetics and high-voltage engineering.

He is a Member of the CIGRÉ Study Committee A3 – High-voltage equipment, IEEE Member since 2012 and ACES Member since 2016.

Ivo Uglešić was born in Zagreb, Croatia, in 1952. He received his Ph.D. degree in Electrical Engineering and Computing from the University of Zagreb, Croatia, in 1988.

Currently, he is a Professor at the Faculty of Electrical Engineering and Computing (Department of Energy and Power systems), University of Zagreb. He is the Head of the High-Voltage Laboratory at the Faculty of Electrical Engineering and Computing. His areas of interest include high-voltage engineering and power transmission.

Mladen Vidović was born in Zagreb, Croatia. He received his B.Eng. degree from University of Zagreb, Faculty of Electrical Engineering in 1984.

He has been working in KONČAR Electrical Engineering Institute since 1986, at Switchgear and Controlgear Department where he is currently the Head of Research and Development Section. His areas of interest are design and diagnostic of high-voltage switchgears and development of on-line monitoring systems of high-voltage apparatus. He is the author of several papers and patents.